Carbon 189 (2022) 579–585

Contents lists available at ScienceDirect

Carbon

journal homepage: www.elsevier.com/locate/carbon

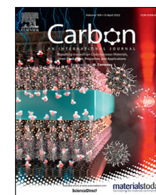

A study of the correlation between the oxidation degree and thickness of graphene oxides

Jaejun Park [a, b, 1], Wonki Lee [a, b, 1], Jungtae Nam [a], Joong Tark Han [c], Chel-Jong Choi [b, **], Jun Yeon Hwang [a, *]

[a] Institute of Advanced Composite Materials, Korea Institute of Science and Technology (KIST), Jeonbuk, 55324, Republic of Korea
[b] School of Semiconductor and Chemical Engineering, Semiconductor Physics Research Center (SPRC), Jeonbuk National University, Jeonju 54896, Republic of Korea
[c] Nano Hybrid Technology Research Center, Electrical Materials Research Division, Korea Electrotechnology Research Institute, Changwon 51543, Republic of Korea

A R T I C L E I N F O

Article history:
Received 28 September 2021
Received in revised form
29 December 2021
Accepted 30 December 2021
Available online 1 January 2022

Keywords:
Graphene oxide
Oxygen functional groups
d-spacing
Thickness

A B S T R A C T

Thickness control is very important to commercial applications of 2D nanomaterials. The thickness of graphene oxide (GO) layers varies depending on the fabrication process, which is directly influenced by the content of oxygen functional groups. The correlation between the thickness and the degree of oxidation in different types of GO samples fabricated by various process are investigated through macroscopic and microscopic analysis. In this experiment, fabricated differently four GOs having various degree of oxidation were analyzed by X-ray Photoelectron Spectroscopy (XPS) to evaluate the degree of oxidation, respectively. A monolayer analysis by Atomic Force Microscope (AFM) and d-spacing analysis by X-ray Diffraction (XRD) and Transmission Electron Microscope (TEM) were employed to compare and analyze the effect of the degree of oxidation on the thickness of the GO layers. The results showed that the degree of oxidation had a directly proportional relationship with the thickness and d-spacing of the specimens. Raman spectroscopy was also employed to further verify the proportional relationship between the degree of oxidation and the thickness of the GO specimens. The degree of oxidation of GO is to approximate by the analysis using the Raman spectroscopy, XRD and TEM results.
© 2022 Elsevier Ltd. All rights reserved.

1. Introduction

Recently, graphene has been increasingly studied as a promising candidates for electrodes, sensors, and energy industries due to its excellent mechanical and electrical characteristics [1–9]. So, the most basic and important thing in the study of graphene applications is to measure and evaluate its material properties. For study graphene is usually prepared in three forms: flakes, films and powders [10]. Among them, graphene, in powder form, is hydrophobic and tends to stack and agglomerate by π bonds in the matrix, thereby exhibiting low dispersibility in the solution. To improve the dispersibility, it can be addressed by oxidizing graphene. Graphene oxide (GO) has hydrophilic properties by oxygen functional groups introduced between surfaces in the solution, thereby inducing delamination between layers [11,12]. To be able to accurately determine the physical properties of GOs, it is necessary of precise thickness measurement of the GO.

While the graphene thickness is usually measured by Atomic Force Microscope (AFM), X-ray Diffraction (XRD) and Transmission Electron Microscope (TEM), the GOs are challenging for them [13–15]. This is because a GO has a varying thickness depending on the various fabrication process conditions, and its crystallinity is inferior to Chemical Vapor Deposition (CVD) graphene, and thus it is more difficult to accurately determine the number of layers by typical methods. In addition, the density of defect is increased as much as the graphene is oxidized [16–18]. This leads to chemical composition and structural changes, thus causing the graphene to lose its electrical characteristics. For this reason, it is difficult to directly compare the characteristics of GO and graphene in a standardized manner. The present study has been investigated in order to determine the correlation between the oxidation degree

* Corresponding author.
** Corresponding author.
E-mail addresses: cjchoi@jbnu.ac.kr (C.-J. Choi), junyeon.hwang@kist.re.kr (J.Y. Hwang).
[1] These authors are equally contributed for this work.

https://doi.org/10.1016/j.carbon.2021.12.101
0008-6223/© 2022 Elsevier Ltd. All rights reserved.

and the thickness of GOs fabricated by various methods, which contributes to evaluate the various GOs and their commercial applications. Indeed, this is the first direct observation of oxidation degree and thickness on the different types of GOs, which give rise to grasp study on the structure-property relationship of commercialized GO samples.

In this experiment, fabricated differently four types of GOs consequently analyzed quantitatively by XPS to evaluate variations in their chemical composition [19]. And the Fourier Transform Infrared (FT-IR) was measured to increase the reliability of deconvolution in XPS C1s data [19]. The corresponding structural changes were then evaluated by XRD, TEM, AFM, and Raman spectroscopy [20–24]. AFM is a basic analysis method for measuring the roughness or thickness of 2D materials. Therefore, AFM was used to measure the thickness of a monolayer in the thickness assessment of GOs [25]. Among these analytical methods, the XRD analysis involved an issue to be resolved. To date, it has not been clearly established whether the XRD diffraction plane of GO corresponds to the (001) or (002) plane. So, on this issue, in the present study, we clarify the diffraction aspects derived from XRD pattern analysis by comparing the data obtained from XRD patterns and TEM images. In addition to AFM, XRD, and TEM, Raman spectroscopy is complementary method for measuring the thickness of graphene. When measuring the thickness of graphene by Raman spectroscopy, the I_{2D}/I_G ratio is used based on the intensity ratio of the 2D peak to the G peak. Interestingly, the 2D peak of GO has an almost negligible intensity, and thus it can be replaced by the Si peak, which results from the Si substrate. For such a reason, the thickness of GOs is measured based on the I_G/I_{Si} ratio [26,27]. Likewise, the I_G/I_{Si} ratio of GOs was measured by Raman spectroscopy, the d-spacing was determined by XRD and TEM, and the O/C ratio was analyzed by X-ray Photoelectron Spectroscopy (XPS), and it was found that the measured I_G/I_{Si} ratio and d-spacing were proportional to the measured O/C ratio. These results mean that if a database of measurement and analysis of GOs is accumulated, the remaining data can be predicted with only one data of these equipment.

2. Experimental

Four types of GOs were used in the present study. We named GO 1 to GO 4 in the order of high oxidation degree according to the XPS results conducted later. GO 1 and GO 2 were purchased from Graphene All Co., from South Korea, and GO 3 were purchased from Standard Graphene Co., from South Korea. GO 4 was provided by Korea Electrotechnology Research Institute (KERI). Even though the fabrication methods of these samples are different and veiled, all the experiments were carried out under the same conditions to block the measurement variables. All samples are deionized (DI) water based and GO 1 is 5 mg/ml, pH value is 1.68, GO 2 is 2 mg/ml, pH value is 2.58, GO 3 is 10 mg/ml, pH value is 2.79, GO 4 is 0.02 mg/ml, pH value is 8.17. For each sample, only light portions were collected using a centrifuge, and diluted with DI water to prepare portions to be measured again. We performed sampling to proceed with XPS, AFM, and Raman spectroscopy in series for the same part of each GO specimens. Photo lithography was used to pattern the align marker on a SiO_2/Si substrate. Then, Au was deposited by thermal evaporation. Align markers on the SiO_2/Si substrate recorded the positions of GOs and served as calibrations when measuring XPS. Samples of XPS, AFM, Raman spectroscopy were prepared by dropping and spin-coating the water based GO solution on the pre-patterned substrate. The FT-IR (Thermo Fisher Scientific™·iS10, 24 scan rate, 16 resolution, Absorbance mode) samples were prepared by filtering DI water using a vacuum filter and drying it all day in a dry oven at 100 °C. Consequently, XRD and TEM samples were prepared by sampling a GO powder in the XRD holder and dropping a diluted GO solution on the mash grid, respectively. During keeping and testing the samples, the temperature and humidity were kept at 20 °C and 40%, respectively. After the previous basic sampling, the O/C ratio was analyzed by measuring the C1s peak of the GO specimens by XPS (Thermo Fisher Scientific™ · K-Alpha with a range of 400 μm × 400 μm and a degree of vacuum of 8–9 × 10^{-9}). The degree of oxidation of GO was determined through the O/C ratio derived by XPS, and the measurement and analysis of other following equipment were conducted based on the oxidation degree derived by XPS. The monolayer thickness of the GO with a varying degree of oxidation was measured by AFM (Park systems™ · NX10, Noncontact mode, Cantilever PPP-NCHR with an amplitude of 15 nm, a set point of 10 nm, a scan rate of 0.25 Hz, and a resolution of 39.0625 nm), and the tendency about correlation between the thickness and the degree of oxidation was then showed. To accurately measure the thickness of the GO layers, XRD (Rigaku™ · SmartLab, X-ray with a wavelength of 1.54 Å) pattern analysis was employed so that the correlation between the d-spacing of the GO and the degree of oxidation could be examined. Next, TEM (Thermo Fisher Scientific™ · Titan, HRTEM, 80 kv) images were obtained and analyzed to measure the d-spacing of the GO specimens and then the results were compared with those measured by XRD for consistency. Also, AFM was used to locate three to four layers spots of each GO specimen, and a Raman mapping image analysis was performed on the selected spots to measure the I_G/I_{Si} ratio of the GO specimens by a Raman spectroscopy (Renishaw™ · Invia Reflex with a wavelength of 514.5 nm, a grating of 2400 l/nm, a laser power of 5%, and a mapping step resolution of 0.4 μm and in a static mode). During Raman analysis, the Si signal changes dramatically depending on the type of lens and the power of the laser. We used an objective lens (Leica™ from Germany) with a magnification of 50 for Raman analysis. The laser of the 514 nm wavelength of instrument we used is 8.51 mW at 100%, 4.30 mW at 50%, 863 μW at 10%, and 425 μW at 5% power at the tip of the 50 magnification lens. To check the resolution of Raman spectroscope in this study, a line profile was performed for the peak intensity of Si (I_{si}) signal as shown in Fig. S1. By detecting the signal change of I_{si} on the Au pattern, the laser beam spot size was estimated according to the magnification of the lens and the laser power. For this evaluation test of spot size, it is only suitable to use 50×. The details of spot size and magnification based on laser power were presented at Table S1. Finally, the I_G/I_{Si} ratio of the GOs measured from the Raman mapping images, the d-spacing data obtained from the XRD and TEM results, and the O/C ratio measured by XPS were plotted against each other to analyze their relationship.

3. Results and discussion

The substrates used in this experiment were actually Au-patterned, which contributes to find the GO position during the XPS, AFM and Raman measurement. The XPS test has been carried out to analyze the degree of GO oxidation. C1s spectra of XPS results of the four types of GOs: GO 1, GO 2, GO 3, and GO 4 (Fig. 1) [28]. An area of 400 μm × 200 μm of each specimen was subjected to quantitative analysis of O/C ratios to confirm the oxygen functional groups. In the XPS C1s spectra, each peak corresponds to a specific element combined with constant binding energy and certain error ranges.

We measured FT-IR spectra in the mid-IR range (2000–1000 cm^{-1}) to determine the structures and functional groups present in the GO samples (Fig. 2) [19]. The IR spectrum of GO shows peaks at 1731, 1626, 1381, 1232 and 1059 cm-1, which have been assigned to C=O, C=C, C–OH, C–O–C and C–O, respectively.

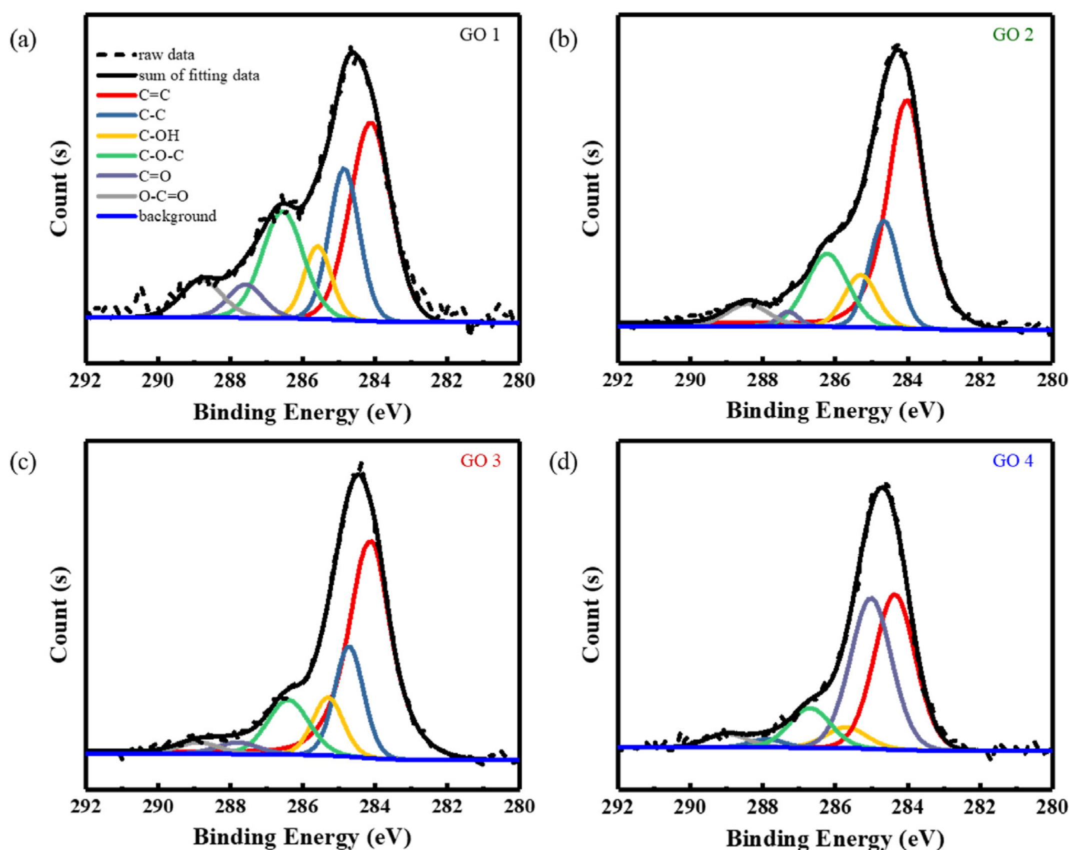

Fig. 1. XPS C1s spectra (The short black dash line is raw data, the solid line is fitting data: the black line is sum of fitted data, the red line is C=C bond, the blue line is C–C bond, the yellow line is C–OH bond, the green line is C–O–C bond, the violet line is C=O bond, the gray line is O–C=O bond) of (a) GO 1, (b) GO 2, (c) GO 3, and (d) GO 4. (A colour version of this figure can be viewed online.)

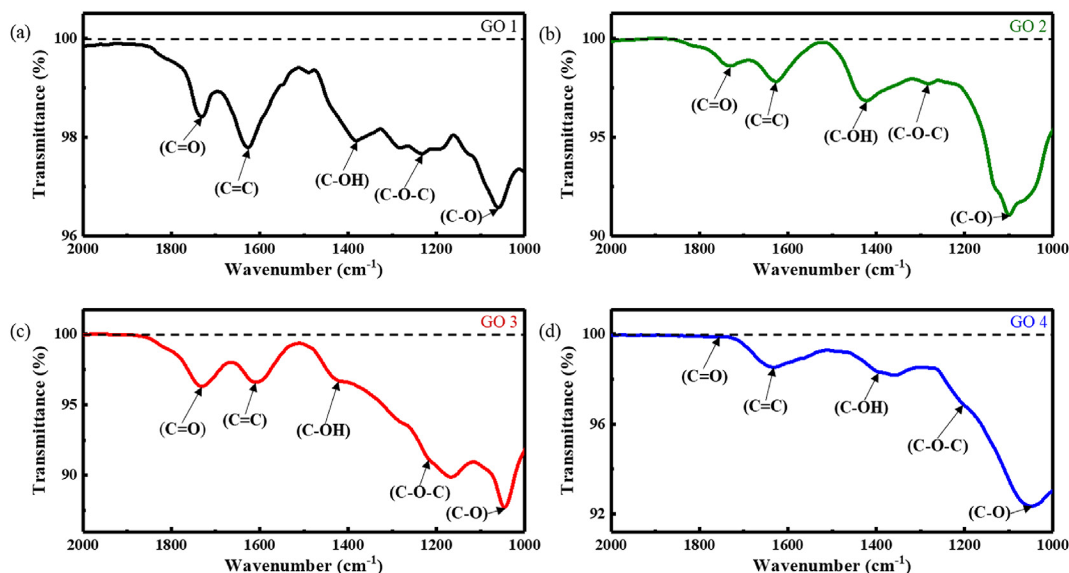

Fig. 2. FT-IR spectra in the range (2000–1000 cm^{-1}) of 4 of (a) GO 1, (b) GO 2, (c) GO 3, (d) GO 4. (A colour version of this figure can be viewed online.)

In the measured XPS spectra, the binding energy of each chemical state was corresponded as follows: 284.2±0.2 eV for the C=C bond, 284.8±0.2 eV for the C–C bond, 285.5±0.2 eV for the C–OH bond, 286.5±0.2 eV for the C–O–C bond, 287.7± 0.2 eV for the C=O bond and 288.8±0.2 eV for the O–C=O bond [29]. To improve the accuracy of the binding energy measurements, it has been by Au (84 eV) as a referred correction, which was placed under each GO specimen [30]. The O/C ratio of each Go was fitted using the following equation (eq. (1)) [31].

Table 1
Atomic percentage, Full Width at Half Maximum and O/C ratio of oxygen functional groups derived from the C1s analysis of four types of GOs, respectively. Except for O/C ratio, all have an error range of 0.05.

	C1s	C=C	C–C	C–OH	C–O–C	C=O	O–C=O	O/C ratio
GO 1	**At (%)**	37.5	20.8	9.0	20.2	5.4	7.1	0.39 ±0.005
	FWHM (eV)	1.4	1.0	0.9	1.4	1.2	1.4	
GO 2	**At (%)**	54.6	15.7	8.6	15.1	1.5	4.6	0.27 ±0.005
	FWHM (eV)	1.3	1.0	1.1	1.4	0.7	1.4	
GO 3	**At (%)**	57.2	16.7	9.3	11.8	2.5	2.5	0.23 ±0.005
	FWHM (eV)	1.4	0.9	1.0	1.4	1.4	1.4	
GO 4	**At (%)**	39.9	39.0	5.5	10.3	1.8	3.6	0.20 ±0.005
	FWHM (eV)	1.3	1.3	1.4	1.4	1.1	1.4	

$$O/_{C}\,ratio = \frac{A_{C-OH} + A_{C=O} + \frac{1}{2}\cdot A_{C-O-C} + 2\cdot A_{O-C=O}}{A_{tot}} \quad (1)$$

In the equation, A is the parameter which indicate Area (P) CPS. The O/C ratio, atomic (%), and FWHM of each GO are shown in Table 1. And, since we performed GO XPS measurements on a SiO_2 substrate, the C1s raw data of the SiO_2 substrate and GO 1 are shown in Fig. S2. It was found that the degree of oxidation was the highest in GO 1 sample and decreased in the order of GO 1, GO 2, GO 3, and GO 4. The O/C ratio measured by XPS experiment is crucial factor to investigate the GO thickness. We focused the correlation between the degree of oxidation and the d-spacing obtained by XRD and TEM. In addition, the GO thickness measured by AFM has been added, and the results obtained by Raman spectroscopy was examined.

In Fig. 3, we presented the comparative analysis of XRD and TEM results in order to accurately analyze the d-spacing of GO. The d-spacing obtained by XRD using the Bragg equation was presented in Table 2. As can be seen from Table 2, we can see that the d-spacing of GO 1 by the (001) plane is 9.69 Å, and the d-spacing of GO 4 is 6.65 Å, which narrows from GO 1 to GO 4. It pointed that the d-spacing was also found to be proportional to the degree of oxidation.

In the XRD pattern analysis, the d-spacing of graphene is calculated using the θ value corresponding to the (001) plane. Actually, what could be the possibly corresponded to the plane of graphene? This is an issue to the GO analysis by XRD measurement. However, it has yet to be clearly established whether the diffraction plane obtained in the XRD pattern analysis of GOs corresponds to

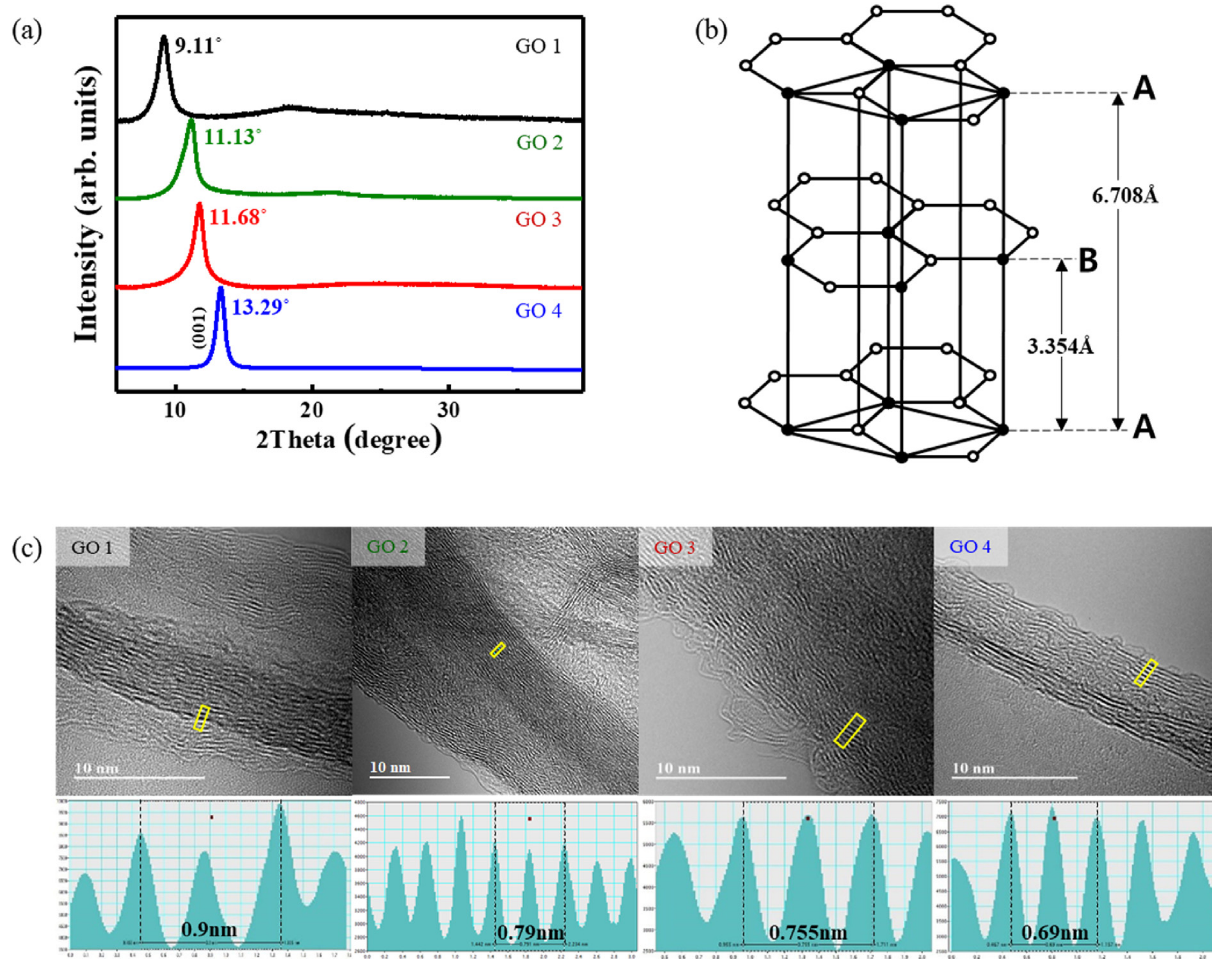

Fig. 3. (a) XRD pattern of four types of GOs, (b) HCP structure of graphite, (c) HRTEM image of four types of GOs. (A colour version of this figure can be viewed online.)

Table 2
The d-spacing data obtained by calculating XRD pattern of Fig. 2(a).

XRD(λ: 1.54)	Peak Pos of (001) (°2θ)	FWHM (°2θ)	*d*-spacing (Å)
GO 1	9.11	1.00	9.69
GO 2	11.13	1.12	7.94
GO 3	11.68	0.96	7.57
GO 4	13.29	0.81	6.65

the (002) or (001) plane. In the present study, the d-spacing measured by XRD analysis was analyzed and compared with that measured from the TEM images, and it was concluded that the obtained XRD diffraction plane of the GO specimens corresponded to the (001) plane. It is supported by the fact that the d-spacing derived by TEM images was half compared with XRD values (Fig. 3(a, c)). The observation of the (001) plane, instead of the (002) plane, in GOs can be explained as follows. In general, bulk graphene has an HCP crystalline structure, which involves an AB stacking sequence in which layer A and layer B are stacked alternately (Fig. 3(b)) [32]. However, when graphene is oxidized, its unique structure easily collapses. For this reason, the (002) plane found in the graphene bulk structure is not found in GO. Instead, it is typically found as (001) plane in GO.

Next, the monolayer thickness of each GO specimen was measured by AFM to examine the effect of the content of the oxygen functional groups on the monolayer thickness (Fig. 4). Aside from the AFM mapping images shown in Fig. 4, the measurement was repeated four to five times for each specimen. The results also showed a similar trend with the O/C ratio measured by XPS. This confirms that the presence of the oxygen functional groups has a critical effect on increasing the thickness of GOs. However, measuring the monolayer thickness of the GO on the substrate may give a different result from measuring the monolayer thickness of the GO monolayer on top of another GO. To confirm this, the thickness of the folded part of GO 1, 2, 3 was further analyzed (Fig. 4). It was found that the monolayer thickness of the GO on the substrate was not equal to the monolayer thickness of the GO on top of another GO. For example, looking at the histogram [33,34] corresponding to the image of GO 1 in Fig. 4(a), monolayer GO is 1.044 nm from the substrate and monolayer GO is 0.889 nm from another GO. The difference between them is about 0.15 nm. It can be seen that GO 2 and GO 3 also have thinner thickness on GO than on substrate. In addition, in order to demonstrate the thickness change of GO samples according to the pH value, the thickness measurement by AFM was performed on the GO samples at the pH level 6.5 by adjusting the GO concentration in the solution. The results of the experiment confirmed no significant thickness change based on the pH level. For examples, the thickness of monolayer GO1 sample has 1.042 nm at pH level 3.93, while the thickness is 1.037 nm at pH level 6.5. The comparison of thickness by AFM experiment was shown at Fig. S3.

However, the most significant limitation of the AFM analysis is that while the method provides a relative comparison of the thickness of GOs, along with the trend in thickness variations, it is less effective in accurately measuring their thickness. For example, the monolayer thickness of pristine graphene is measured to be about 0.335 nm by AFM. However, when measured by AFM, the monolayer thickness of GOs is greater than the typical value. This inconsistency is attributed to the interaction between the tip and the specimen surface, relevant surface chemistry, etc [35]. This inconsistency issue may further lead to a suspicion that any layer that has been confirmed to be a monolayer may not be a single layer in reality.

Fig. 5 shows the relationship between the thickness and the Raman spectra of the GO specimens. AFM mapping images of three-to four-layered parts of the four GO specimens, GO 1, 2, 3, and 4 (Fig. 5(a)). These three-to four-layered parts were selected based on a contrast difference in optical microscope images. Fig. 5(b) presents the I_G/I_{Si} ratio determined based on the Raman mapping images about the same parts (Fig. 5(a)). Typically, when evaluating the number of layers on GO using Raman, evaluation is performed using the I_{2D}/I_G ratio. However, in the case of GO, the double-resonance phenomenon of phonon in the 2D band of graphene is rarely measured due to defects such as oxygen functional groups. Therefore, instead of the I_{2D}/I_G ratio, the number of GO layers was analyzed by the I_G/I_{Si} ratio using the Si peak appearing on the substrate. The reason for using the I_G/I_{Si} ratio to evaluate the number of layers of GO is as follows. In order for the Raman spectrum to obtain a Si signal from the SiO_2 substrate, it must pass through GO layers to obtain a signal for Raman detector. As the signal is transmitted through the GO, the intensity of the Si peak decreases due to scattering. Consequently, the intensity of Si peak is diminished by the number of layers and the oxidation degree of GO samples. This proves that the I_G/I_{Si} ratio have determined the number of layers of GO with respect to the degree of oxidation [26,27]. The observation has been shown at Fig. 5(c) in terms of $I_G/$

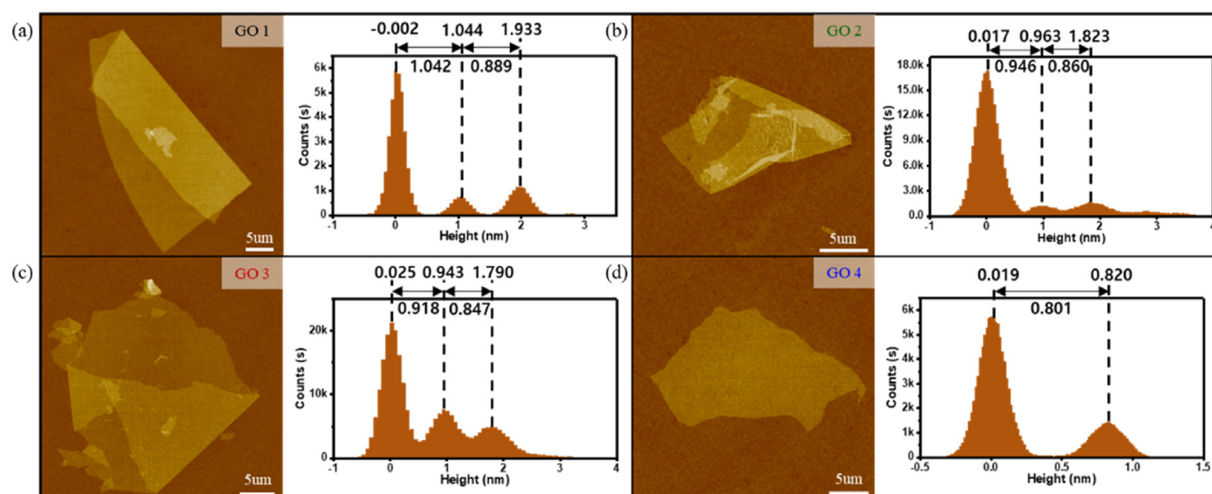

Fig. 4. NCM(Non-Contact Mode) AFM topography and histogram of the folded monolayer of (a) GO 1, (b) GO 2, (c) GO 3, and the monolayer of (d) GO 4 to show differences in thickness of GO according to degree of oxidation. (A colour version of this figure can be viewed online.)

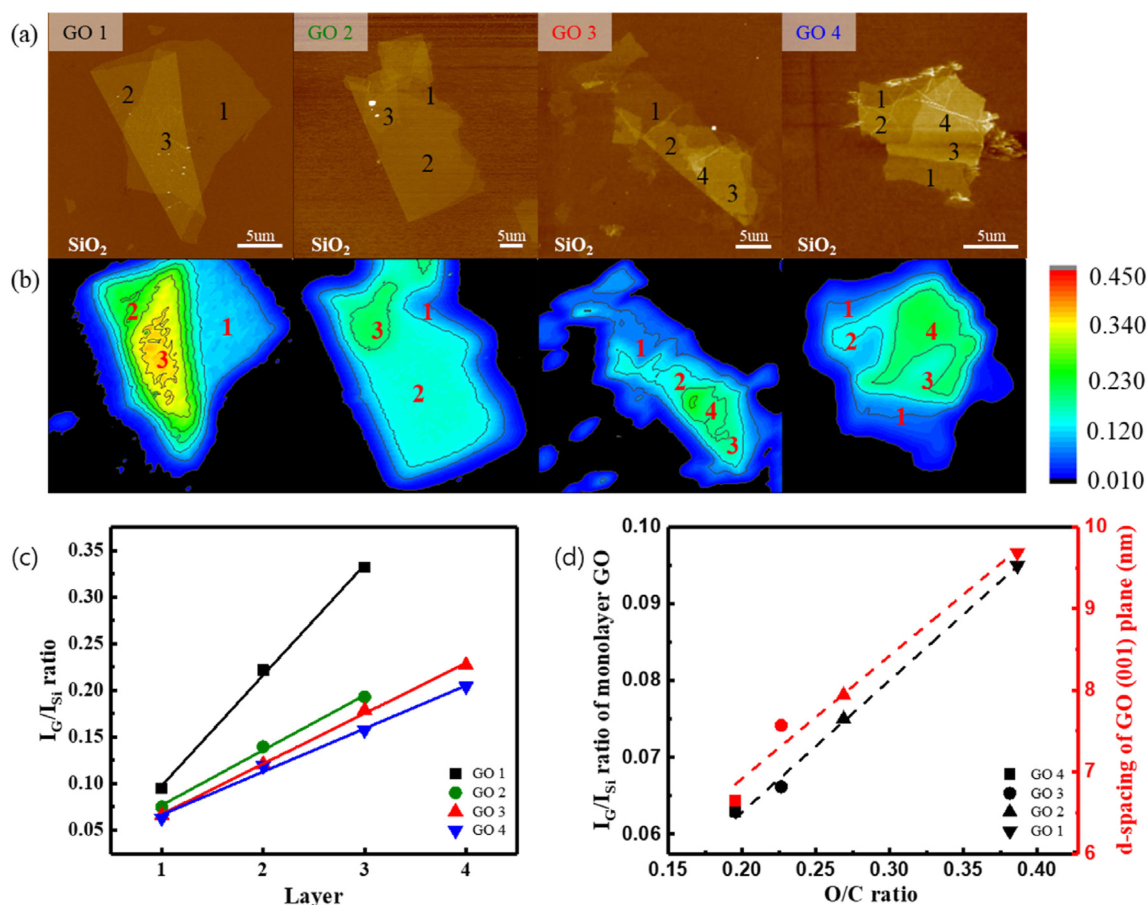

Fig. 5. (a) AFM mapping image of four types of three-to four-layers GOs, (b) Raman mapping image of four types of three-to four-layers GOs that the same region as the AFM image of (a), (c) The scatter graph about layer of four types of GOs vs Intensity ratios of the G band over the Si peak of four types of GOs. The data in the graph are average data, and each error range is within 0.01, (d) The scatter graph about O/C ratio of four types of GOs vs Intensity ratios of the G band over the Si peak of four types of GOs & d-spacing of four types of GOs. (A colour version of this figure can be viewed online.)

I_{Si} ratio according to the degree of oxidation and the number of layers of GO.

We confirm the I_G/I_{Si} ratio is linearly proportional to the layer number. The slopes of the curves were 0.1136, 0.0590, 0.0541, and 0.0465 for GO 1, GO 2, GO 3, and GO 4, respectively. It was clearly observed that a greater slope corresponded to a higher degree of oxidation. Fig. 5(d) shows the relationship between the O/C ratio of each GO specimen and the I_G/I_{Si} ratio and d-spacing of the GO monolayers. Both the I_G/I_{Si} ratio and d-spacing of the GO monolayers were found to be linearly proportional to O/C ratio. The slope of the I_G/I_{Si} ratio curve was 0.0021, and the slope of the d-spacing curve was 0.0944. Here, each of the plotted d-spacing values was obtained from the (001) plane measured in the XRD analysis. These results confirm that, even if the degree of oxidation of GOs is unknown, it is likely to approximate the O/C ratio by measuring their I_G/I_{Si} ratio by Raman spectroscopy and determining the d-spacing of the GO monolayers by XRD and TEM (see Fig. 4(d)). The Raman full scan spectrum of each GO samples is shown in Fig. S4, and the peak positions and FWHM values of each GO are shown in Table S2.

4. Conclusions

In summary, the thickness of GO varies depending on the O/C ratios. The d-spacing of GO is proportional to the degree of oxidation. The comparison of the d-spacing measurements by TEM and XRD confirmed that the obtained diffraction plane of each GO specimen corresponded to the (001) plane. Also, Raman mapping was applied to three-to four-layered GO specimens, and it was found that their thickness could be determined by measuring their I_G/I_{Si} ratios. Moreover, both the I_G/I_{Si} ratio and the d-spacing were found to be proportional to the O/C ratios measured by XPS. The O/C ratios of GO samples are rationally predicted by determining the I_G/I_{Si} ratio and d-spacing of the corresponding GO. The understanding of the correlation between degree of oxidation and thickness of GO through the proposed methodology is the effective way to perceive the structure-property relationship of commercialized GO samples.

CRediT authorship contribution statement

Jaejun Park: Formal analysis, Writing – original draft, characterized, measured and analyzed mateirals and wrote the manuscript. **Wonki Lee:** Formal analysis, Writing – original draft, characterized, measured and analyzed mateirals and wrote the manuscript. **Jungtae Nam:** Formal analysis, Writing – original draft, characterized, measured and analyzed mateirals and wrote the manuscript. **Joong Tark Han:** fabricateed the materials. **Chel-Jong Choi:** Formal analysis, Writing – original draft, Supervision, organized the experiments, supervised the measurement and analysis of mateirals and wrote the manuscript. **Jun Yeon Hwang:** Formal analysis, Writing – original draft, Supervision, organized the experiments, supervised the measurement and analysis of mateirals and wrote the manuscript.

Declaration of competing interest

The authors declare that they have no known competing financial interests or personal relationships that could have appeared to influence the work reported in this paper.

Acknowledgements

This research was supported by the Carbon Industry Ecosystem Creation and Diffusion Program_6 Major Carbon Materials Field International & National Standards Development & Dissemination Project (2M35940) funded by the Ministry of Trade, Industry & Energy and partially from Nano·Material Technology Development Program (NRF-2016M3A7B4900135) through the NRF from Korea government.

Appendix A. Supplementary data

Supplementary data to this article can be found online at https://doi.org/10.1016/j.carbon.2021.12.101.

References

[1] H. Park, S. Chang, X. Zhou, J. Kong, T. Palacios, S. Gradecak, Flexible grapehe electrode-based photovoltaics with record-high efficiency, Nano Lett. 14 (9) (2014) 5148–5154, https://doi.org/10.1021/nl501981f.
[2] S.-H. Bae, Y. Lee, B.K. Sharma, H.-J. Lee, J.-H. Kim, J.-H. Ahn, Graphene-based transparent strain sensor, Carbon 51 (2013) 236–242, https://doi.org/10.1016/j.carbon.2012.08.048.
[3] D. Wei, J. Kivioja, Graphene for energy solutions and its industrialization, Nanoscale 5 (21) (2013) 10108–10126, https://doi.org/10.1039/C3NR03312K.
[4] R.R. Raj, J. Yoganandh, M.S.S. Saravanan, S.S. Kumar, Effect of graphene addition on the mechanical characteristics of AA7075 aluminium nanocomposites, Carbon Lett. 31 (1) (2020) 125–136, https://doi.org/10.1007/s42823-020-00157-7.
[5] T.-J. Ha, J. Lee, S.K.F. Chowdhury, D. Akinwande, P.J. Rossky, A. Dodabalapur, Transformation of the electrical characteristics of graphene field-effect transistors with fluoropolymer, ACS Appl. Mater. Interfaces 5 (1) (2013) 16–20, https://doi.org/10.1021/am3025323.
[6] D.G. Papageorgiou, I.A. Kinloch, R.J. Young, Mechanical properties of graphene and graphene-based nanocomposties, Prog. Mater. Sci. 90 (2017) 75–127, https://doi.org/10.1016/j.pmatsci.2017.07.004.
[7] T. Cusati, G. Fiori, A. Gahoi, V. Passi, M.C. Lemme, A. Fortunelli, G. Iannaccone, Electrical properties of graphene-metal contacts, Sci. Rep. 7 (1) (2017) 5109, https://doi.org/10.1038/s41598-017-05069-7.
[8] Y. Zhu, S. Murali, W. Cai, X. Li, J.W. Suk, J.R. Potts, R.S. Ruoff, Graphene and graphene oxide: synthesis, properties, and applications, Adv. Mater. 22 (35) (2010) 3906–3924, https://doi.org/10.1002/adma.201001068.
[9] J. Nam, I. Lee, D.Y. Lee, M. Kim, K.S. Kim, Abnormal grain growth for single-crystal Cu substrate and chemical vapor deposition of graphene on it, J. Kor. Phys. Soc. 76 (10) (2020) 923–927.
[10] D.K. James, J.M. Tour, Graphene: powder, flakes, ribbons, and sheets, Acc. Chem. Res. 46 (10) (2012) 2307–2318, https://doi.org/10.1021/ar300127r.
[11] J.W. Suk, R.D. Piner, J. An, R.S. Ruoff, Mechanical properties of monolayer graphene oxide, ACS Nano 4 (11) (2010) 6557–6564, https://doi.org/10.1021/nn101781v.
[12] C.J. Shearer, A.D. Slattery, A.J. Stapleton, J.G. Shapter, C.T. Gibson, Accurate thickness measurement of graphene, Nanotechnology 27 (12) (2016) 125704–125713, https://doi.org/10.1088/0957-4484/27/12/125704.
[13] P. Nemes-Incze, Z. Osvath, K. Kamaras, L.P. Biro, Anomalies in thickness measurement of graphene and few layer graphite crystals by tapping mode atomic force microscopy, Carbon 46 (2008) 1435–1442, https://doi.org/10.1016/j.carbon.2008.06.022.
[14] K.S. Novoselov, D. Jiang, F. Schedin, T.J. Booth, V.V. Khotkevich, S.V. Morozov, A.K. Geim, Two-dimensional atomic crystals, Proc. Natl. Acad. Sci. Unit. States Am. 102 (30) (2005) 10451–10453, https://doi.org/10.1073/pnas.0502848102.
[15] O. Monticelli, Z. Musina, S. Russo, S. Bals, On the use of TEM in the characterization of nanocomposites, Mater. Lett. 61 (16) (2007) 3446–3450, https://doi.org/10.1016/j.matlet.2006.11.086.
[16] J. Guerrero-Contreras, F. Caballero-Briones, Graphene oxide powders with different oxidation degree, prepared by synthesis variations of the Hummers method, Mater. Chem. Phys. 153 (2015) 209–220, https://doi.org/10.1016/j.matchemphys.2015.01.005.
[17] D. Voiry, J. Yang, J. Kupferberg, R. Fullon, C. Lee, H.Y. Jeong, H.S. Shin, M. Chhowalla, High-quality graphene via microwave reduction of solution-exfoliated graphene oxide, Science 353 (6306) (2016) 1413–1416, https://doi.org/10.1126/science.aah3398.
[18] Y. Chen, Y. Niu, T. Tian, J. Zhang, Y. Wang, Y. Li, L.-C. Qin, Microbial reduction of graphene oxide by Azotobacter chroococcum, Chem. Phys. Lett. 677 (2017) 143–147, https://doi.org/10.1016/j.cplett.2017.04.002.
[19] K. Krishnamoorthy, M. Veerapandian, K. Yun, S.-J. Kim, The chemical and structural analysis of graphene oxide with different degrees of oxidation, Carbon 53 (2013) 38–49, https://doi.org/10.1016/j.carbon.2012.10.013.
[20] L. Stobinski, B. Lesiak, A. Malolepszy, M. Mazurkiewicz, B. Mierzwa, J. Zemek, P. Jiricek, I. Bieloshapka, Graphene oxide and reduced graphene oxide studied by the XRD, TEM and electron spectroscopy methods, J. Electron. Spectrosc. Relat. Phenom. 195 (2014) 47–57, https://doi.org/10.1016/j.elspec.2014.07.003.
[21] L.M. Malard, M.A. Pimenta, G. Dresselhaus, M.S. Dresselhaus, Raman spectroscopy in graphene, Phys. Rep. 473 (5–6) (2009) 51–87, https://doi.org/10.1016/j.physrep.2009.02.003.
[22] A.C. Ferrari, J. Robertson, Interpretation of Raman spectra of disordered and amorphous carbon, Phys. Rev. B 61 (20) (2000) 47–57, https://doi.org/10.1103/PhysRevB.61.14095.
[23] A.C. Ferrari, Raman spectroscopy of graphene and graphite: disorder, electron-phonon coupling, doping and nonadiabatic effects, Solid State Commun. 143 (1–2) (2007) 47–57, https://doi.org/10.1016/j.ssc.2007.03.052.
[24] Y.y. Wang, Z.H. Ni, T. Y, Z.X. Shen, H.M. Wang, Y.H. Wu, W. Chen, A.T.S. Wee, Raman studies of monolayer graphene the substrate effect, J. Phys. Chem. C 112 (29) (2008) 10637–10640, https://doi.org/10.1021/jp8008404.
[25] F. Rui, L. Ying, G. Xueping, D. Ming, L. Shubiao, L. Tianyu, L. Zhi, Preparation and photocatalytic degradation activity of TiO_2/rGO/polymer composites, Colloid Polym. Sci. 293 (4) (2015) 1151–1157, https://doi.org/10.1007/s00396-015-3507-x.
[26] Y.-S. No, H.K. Choi, J.-S. Kim, H. Kim, Y.-J. Yu, C.-G. Choi, J.S. Choi, Layer number identification of CVD-grown multilayer graphene using Si peak analysis, Sci. Rep. 8 (1) (2018) 571–579, https://doi.org/10.1038/s41598-017-19084-1.
[27] D. Kostiuk, M. Bodik, P. Siffalovic, M. Jergel, Y. Halahovets, M. Hodas, M. Pelletta, M. Pelach, M. Hulman, Z. Spitalsky, M. Omastova, E. Majkova, Reliable determination of the few-layer graphene oxide thickness using Raman spectroscopy, J. Raman Spectrosc. 47 (2016) 391–394, https://doi.org/10.1002/jrs.4843.
[28] G.H. Major, T.G. Avval, B. Moeini, G. Pinto, D. Shah, V. Jain, V. Carver, W. Skinner, T.R. Gengenbach, C.D. Easton, A. Herrera-Gomez, T.S. Nunney, D.R. Baer, M.R. Linford, Assessment of the frequency and nature of erroneous x-ray photoelectron spectroscopy analyses in the scientific literature, J. Vac. Sci. Technol. 38 (6) (2020) 61204–61216, https://doi.org/10.1116/6.0000685.
[29] M. Smith, L. Scudiero, J. Espinal, J.-S. McEwen, M. Garcia-Perez, Improving the deconvolution and interpretation of XPS spectra from chars by ab initio calculations, Carbon 110 (2016) 47–57, https://doi.org/10.1016/j.carbon.2016.09.012.
[30] I.S. Zhidkov, E.Z. Kurmaev, S.O. Cholakh, E. Fazio, L. D'Urso, XPS study of interactions between linear carbon chains and colloidal Au nanoparticles, Mendeleev Commun. 30 (2020) 285–287, https://doi.org/10.1016/j.mencom.2020.05.027.
[31] A. Kovtun, D. Jones, S. Dell'Elce, E. Treossi, A. Liscio, V. Palermo, Accurate chemical analysis of oxygenated graphene-based materials using X-ray photoelectron spectroscopy, Carbon 143 (2019) 268–275, https://doi.org/10.1016/j.carbon.2018.11.012.
[32] J. Lin, W. Fang, W. Zhou, A.R. Lupini, J.C. Idrobo, J. Kong, S.J. Pennycook, S.T. Pantelides, AC/AB stacking boundaries in bilayer graphene, Nano Lett. 13 (2007) 3262–3268, https://doi.org/10.1021/nl4013979.
[33] H.R. Thomas, S.P. Day, W.E. Woodruff, C. Valles, R.J. Young, I.A. Kinloch, G.W. Morley, J.V. Hanna, N.R. Wilson, J.P. Rourke, Deoxygenation of graphene oxide: reduction or cleaning? Chem. Mater. 25 (2013) 3580–3588, https://doi.org/10.1021/cm401922e.
[34] X. Diez-Betriu, F.J. Mompean, C. Munuera, J. Rubio-Zuazo, R. Menendez, G.R. Castro, A. de Andres, Graphene-oxide stacking and defects in few-layer films: impact of thermal and chemical reduction, Carbon 80 (2014) 40–49, https://doi.org/10.1016/carbon.2014.08.016.
[35] K.A. Mkhoyan, A.W. Contryman, J. Silcox, D.A. Stewart, G. Eda, C. Mattevi, S. Miller, M. Chholwalla, Atomic and electronic structure of graphene-oxide, Nano Lett. 9 (2009) 1058–1063, https://doi.org/10.1021/nl8034256.